IOPscience iopscience.iop.org

Home Search Collections Journals About Contact us My IOPscience

Current ramps in tokamaks: from present experiments to ITER scenarios

This article has been downloaded from IOPscience. Please scroll down to see the full text article.

2011 Nucl. Fusion 51 083026

(http://iopscience.iop.org/0029-5515/51/8/083026)

View the table of contents for this issue, or go to the journal homepage for more

Download details:
IP Address: 194.81.223.66
The article was downloaded on 27/07/2012 at 15:40

Please note that terms and conditions apply.

Nucl. Fusion **51** (2011) 083026 (11pp) doi:10.1088/0029-5515/51/8/083026

Current ramps in tokamaks: from present experiments to ITER scenarios

F. Imbeaux[1], J. Citrin[2], J. Hobirk[3], G.M.D. Hogeweij[2], F. Köchl[4], V.M. Leonov[5], S. Miyamoto[6], Y. Nakamura[7], V. Parail[8], G. Pereverzev[3], A. Polevoi[9], I. Voitsekhovitch[8], V. Basiuk[1], R. Budny[10], T. Casper[9], J. Fereira[11], A. Fukuyama[12], J. Garcia[1], Y.V. Gribov[9], N. Hayashi[6], M. Honda[6], I.H. Hutchinson[13], G. Jackson[14], A.A. Kavin[15], C.E. Kessel[10], R.R. Khayrutdinov[5], C. Labate[16], X. Litaudon[1], P.J. Lomas[8], J. Lönnroth[17], T. Luce[14], V.E. Lukash[5], M. Mattei[18], D. Mikkelsen[10], I. Nunes[5], Y. Peysson[1], P. Politzer[10], M. Schneider[1], G. Sips[19], G. Tardini[3], S.M. Wolfe[13], V.E. Zhogolev[5], ASDEX Upgrade Team, C-Mod Team, DIII-D Team, JET-EFDA contributors[a], JT-60U Team, Tore Supra Team, contributors of the EU-ITM ITER Scenario Modelling group, ITPA 'Integrated Operation Scenarios' group members and experts and ITPA 'Transport and Confinement' group members and experts

[1] CEA, IRFM, F-13108 Saint Paul Lez Durance, France
[2] FOM Institute for Plasma Physics Rijnhuizen, Association EURATOM-FOM, Nieuwegein, The Netherlands
[3] Max-Planck-Institut für Plasmaphysik, EURATOM-Assoziation, Garching, Germany
[4] Association EURATOM-ÖAW/ATI, Vienna, Austria
[5] RRC 'Kurchatov Institute', Moscow, Russia
[6] Japan Atomic Energy Agency, 801-1, Mukouyama, Naka, Ibaraki-ken 311-0193, Japan
[7] Nippon Advanced Technology Co., Ltd. Tokai, Ibaraki 319-1112 Japan
[8] EURATOM/CCFE Fusion Association, Culham Science Centre, Abingdon OX14 3DB UK
[9] ITER Organization, Route de Vinon sur Verdon, F-13115 St Paul lez Durance, France
[10] Princeton Plasma Physics Laboratory, PO Box 451, Princeton, NJ USA
[11] Association Euratom-IST, Lisboa, Portugal
[12] Kyoto University, Sakyo-ku, Kyoto 606-8501, Japan
[13] Plasma Science and Fusion Center, MIT, Cambridge, MA, USA
[14] General Atomics, San Diego, USA
[15] NIIEFA, St. Petersburg, Russia
[16] Associazione ENEA/CREATE, DIMET, Università di Reggio Calabria Via Graziella, 89100, Calabria, Italy
[17] Association EURATOM-TEKES, Helsinki University of Technology, Finland
[18] Associazione ENEA/CREATE, DIAM, Seconda Università di Napoli Via Roma 29, 81031, Aversa, Italy
[19] EFDA CSU, JET, UK

E-mail: frederic.imbeaux@cea.fr

Received 25 December 2010, accepted for publication 16 June 2011
Published 14 July 2011
Online at stacks.iop.org/NF/51/083026

Abstract
In order to prepare adequate current ramp-up and ramp-down scenarios for ITER, present experiments from various tokamaks have been analysed by means of integrated modelling in view of determining relevant heat transport models for these operation phases. A set of empirical heat transport models for L-mode (namely, the Bohm–gyroBohm model and scaling based models with a specific fixed radial shape and energy confinement time factors of $H_{96-L} = 0.6$ or $H_{IPB98} = 0.4$) has been validated on a multi-machine experimental dataset for predicting the l_i dynamics within

[a] See the appendix of F. Romanelli *et al* 2010 *IAEA FEC 2010* paper OV/1-3.

 © 2011 IAEA, Vienna Printed in the UK & the USA

±0.15 accuracy during current ramp-up and ramp-down phases. Simulations using the Coppi–Tang or GLF23 models (applied up to the LCFS) overestimate or underestimate the internal inductance beyond this accuracy (more than ±0.2 discrepancy in some cases). The most accurate heat transport models are then applied to projections to ITER current ramp-up, focusing on the baseline inductive scenario (main heating plateau current of $I_p = 15$ MA). These projections include a sensitivity study to various assumptions of the simulation. While the heat transport model is at the heart of such simulations (because of the intrinsic dependence of the plasma resistivity on electron temperature, among other parameters), more comprehensive simulations are required to test all operational aspects of the current ramp-up and ramp-down phases of ITER scenarios. Recent examples of such simulations, involving coupled core transport codes, free-boundary equilibrium solvers and a poloidal field (PF) systems controller are also described, focusing on ITER current ramp-down.

(Some figures in this article are in colour only in the electronic version)

1. Introduction

The scenario design of a future tokamak device naturally focuses on the main heating phase, where fusion reactions take place. Nevertheless, the conditions to access, and eventually to terminate smoothly, the desired main heating state is also an essential topic. The main heating phase is usually carried out at high plasma current, since in a tokamak high current means high confinement. This current is ramped up from a negligible value just after the plasma breakdown to a plateau value, usually mainly by inductive means. After the main heating phase, the plasma current and energy content must also be ramped down smoothly before stopping the plasma discharge. There are several issues to be addressed during plasma current ramp phases of tokamak operation: magnetohydrodynamic (MHD) activity can take place and lead to early plasma termination, depending on the shape of the plasma current density profile. The design of the poloidal field (PF) system and plasma shape controller must allow ramping up the plasma current while providing stable plasma equilibrium. In addition, a significant amount of magnetic flux is needed to ramp the plasma up inductively, thus the flux consumption during the current ramp is also a key element in the design of the PF system. Finally, the confinement/MHD properties of the final 'main heating' phase depend on the q-profile obtained at the end of the ramp-up and may be optimized by applying additional heating and non-inductive current drive during the current ramp.

Current ramp-down in ITER is also quite a challenging part of plasma operation. Apart from the issue of not exceeding the density limit, a burning plasma is usually in H-mode before the current ramp-down and shall return to L-mode before termination. During the H–L transition the plasma quickly loses energy content, which needs to be properly handled by the vertical stability system.

In order to prepare adequate current ramp-up and ramp-down scenarios for ITER, present experiments from various tokamaks (mainly JET, and also ASDEX Upgrade, Tore Supra) have been analysed by means of integrated modelling in view of determining heat transport models relevant for the current ramp-up and ramp-down phases. The results of these studies are presented (section 2.1) and projections to ITER current ramp-up and ramp-down scenarios are performed (section 2.2), focusing on the baseline inductive scenario (main heating plateau current of $I_p = 15$ MA).

While the heat transport model is at the heart of such simulations (because of the intrinsic dependence of the plasma resistivity on electron temperature, among other parameters), more comprehensive simulations are required to test all operational aspects of the current ramp-up and ramp-down phases of ITER scenarios. Recent examples of such simulations, involving coupled core transport codes, free-boundary equilibrium solvers and a PF system controller are described in section 3.

2. Heat transport studies for current ramp-up

We present here simulations that aim to validate heat transport models on existing experiments, then use the validated models for extrapolation to ITER. The simulations reported in this section solve the one-dimensional (radial direction) fluid transport equations on poloidal magnetic flux (current diffusion equation) and electron and ion heat transport. The radial coordinate used in this section is the square root of the normalized toroidal flux ρ. The equilibrium is calculated consistently with the results of the transport equations, using fixed boundary solvers. When analysing present experiments, the shape of the last closed flux surface (LCFS) prescribed in the simulation is determined from magnetic measurements.

2.1. Validating heat transport models against present current ramp-up experiments

A database of eight discharges, mainly from the JET tokamak, has been selected covering ohmic current ramp-up cases, as well as ramp-up assisted with moderate additional heating (up to a few MW). While JET dominates the dataset, a few experiments from Tore Supra and ASDEX Upgrade have been used as well, in order to test the validity of the models for different machine sizes and plasma shapes, which is quite important in view of extrapolation to ITER. Up to now, this heat transport model validation effort has essentially been conducted by modellers from the ITER Scenario Modelling Group of the European Integrated Tokamak Modelling Task Force (see [1] for a presentation of the first results of this group), using the three major European transport codes, namely ASTRA [2], CRONOS [3] and JETTO [4]. This has been the occasion of detailed code benchmarking, quite useful to detect possible mistakes in simulation parametrization and numerical problems, as well as to verify the details of the implementation of the transport models.

The current diffusion and heat transport equations for the electron and ion channels are solved consistently. The boundary condition for solving the electron heat transport equation is prescribed from the measured temperature in the vicinity of the LCFS. In some cases (LHCD or very

Table 1. Analysis of the impact of parameter uncertainties on the l_i prediction, from simulations of JET shot 71827 (ohmic) with the Bohm/gyro-Bohm model. The impact on l_i is the average change in internal inductance obtained at a given time slice, during the current ramp.

Parameter change	Qualitative consequences	Impact on l_i
Increase T_e, edge by a factor of 3	Lower resistivity, current diffuses slower	−0.05
Increase Z_{eff} by 30%	Higher resistivity, current diffuses faster	+0.06
Increase T_i, edge by a factor of 2	Reduces electron to ion collisional heat exchange → increases T_e	−0.02

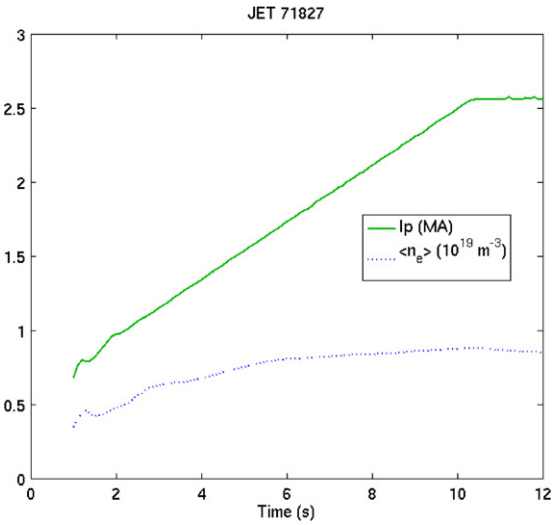

Figure 1. Scenario of JET shot 71827 (ohmic). Time traces of plasma current I_p (green, solid) and volume-averaged electron density $\langle n_e \rangle$ (blue dots).

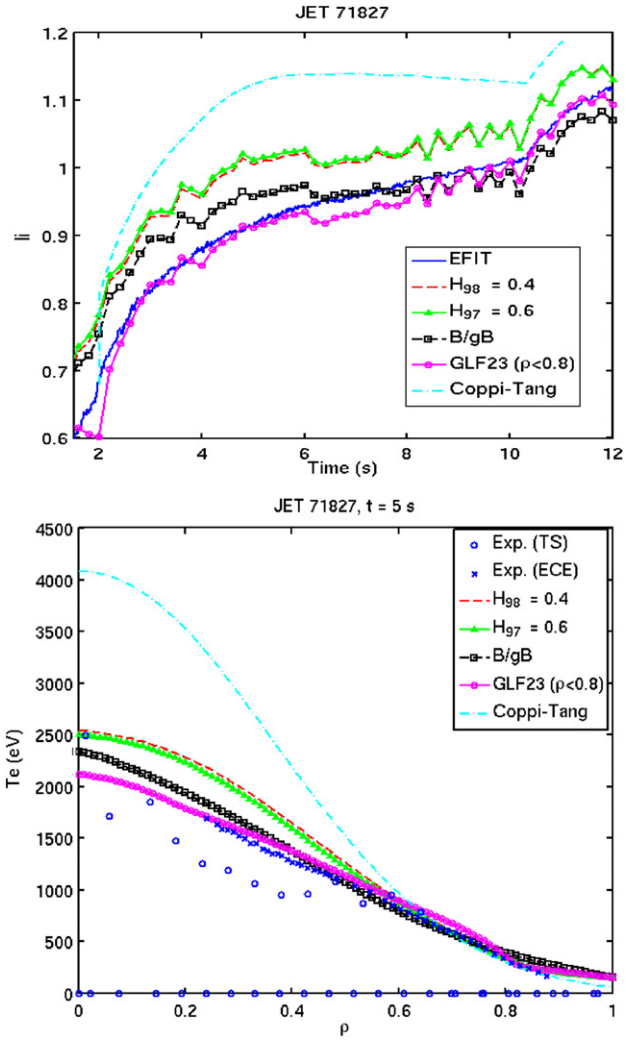

Figure 2. Top: simulation of the internal inductance dynamics of the JET ohmic shot 71827 with several heat transport models. The plasma current is ramped up to 2.5 MA in 10 s. Experimental value (EFIT reconstruction, blue), scaling-based ($H_{98} = 0.4$, red dashed), scaling-based ($H_L = 0.6$, green triangles), Bohm/gyro-Bohm (black squares), GLF23 (applied only inside $\rho = 0.8$ with $\chi_e = \chi_i = 8\,m^2\,s^{-1}$ outside, purple), Coppi–Tang (light blue dash dotted). Bottom: the electron temperature profile at $t = 5$ s. Blue circles and crosses indicate experimental measurements (Thomson scattering and electron cyclotron emission, respectively), the other profiles correspond to the predictions of the models. The same colour code as used for the top figure.

early phases of the discharges), the measurements close to the plasma edge are of poor quality and the uncertainty on the T_e (electron temperature) boundary condition to use is large. This uncertainty influences the absolute internal inductance l_i prediction, depending on the transport model used (typically a difference of 0.05 in l_i is obtained when varying the temperature boundary condition from a factor of 3 for the Bohm–gyroBohm model, the scaling-based models are found less sensitive). In most cases, T_i (ion temperature) measurements are missing and we use $T_i = T_e$ at the boundary. Table 1 presents a quantitative analysis of these uncertainties for one example in our shot database. The electron density profile is prescribed from measurements (Abel inversion of line-integrated interferometer measurements). A flat Z_{eff} profile is assumed, with a uniform value of Z_{eff} prescribed from bremsstrahlung measurements. We also prescribe the radiated power profile from Abel inversion of bolometry measurements, when available. Toroidal rotation is not taken into account. As no or only moderate NBI power was used, plasma rotation is expected to be low and have negligible impact on heat transport. The equilibrium is recalculated using a fixed boundary equilibrium solver, while the dynamics of the plasma boundary are prescribed from pre-existing equilibrium reconstruction constrained by magnetic measurements.

The internal inductance has been chosen as essential parameter/criterion for validation of the heat transport models in the context of current ramp-up and ramp-down phases. Several definitions exist for l_i. In this paper, we choose the one known as $l_i(3)$: $l_i(3) = 2V\langle B_P^2\rangle/(\mu_0 I_P)^2 R_0$ (where V is the plasma volume, I_p the plasma current, R_0 the major radius of the plasma and $\langle\,\rangle$ denotes the average over the whole plasma volume: $\langle B_P^2\rangle = 1/V \int B_P^2\,dV$). This parameter is important from the operational point of view since (i) the range of current profile shapes that can be sustained by the PF coils can be characterized by an interval of l_i; (ii) l_i is a key parameter for the vertical instability; (iii) l_i is also a key parameter for typical magnetohydrodynamical activity during the ramp-up.

Being a normalized volume-averaged quantity, the internal inductance is strongly weighted by the outer half of the plasma. Therefore, details of the current density profile inside

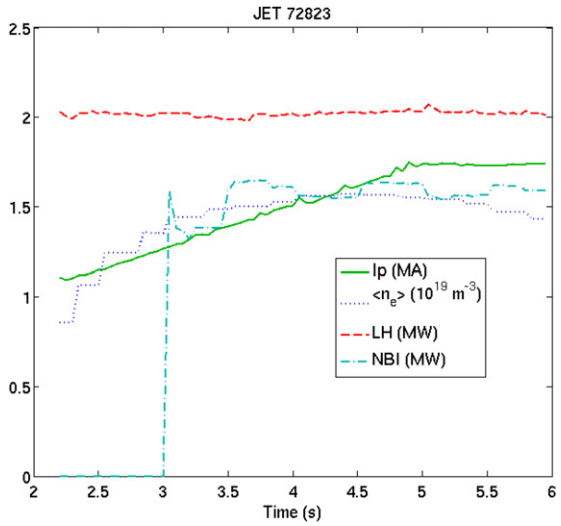

Figure 3. Scenario of JET shot 72823 (LHCD + NBI diagnostic beam). Time traces of plasma current I_p (green, solid), volume-averaged electron density $\langle n_e \rangle$ (dark blue dots), LH power (red dashed) and NBI (light blue dashed dot).

mid-radius have a weak impact on the l_i value. The prediction of l_i dynamics depends essentially on the electron temperature profile outside mid-radius. Even if the heat transport model deviates from the T_e measurements inside mid-radius, or is not accurate on the ion temperature prediction, it may be judged relevant for the prediction of this key operational parameter.

The models tested are the following.

- Scaling-based models, using a fixed radial shape $\chi(\rho, t) = A(t)(1 + 6\rho^2 + 80\rho^{20})$. This shape is relatively flat throughout the plasma core, then presents a rapid increase in the diffusivity close to the LCFS, reproducing the general trend deduced from interpretative analysis of the our ramp-up experimental dataset. The time-dependent factor $A(t)$ is adjusted at each call of the model in order that the plasma thermal energy content W_{th} follows a known scaling expression, namely: $W_{th} = H\tau_E(P_{loss} - \dot{W}_{th})$. In this expression, $\dot{W}_{th}$ denotes the time derivative of W_{th} and P_{loss} the power lost through the separatrix. Two scaling expressions for the energy confinement time τ_E have been used: the ITER96-L (L-mode) [5] scaling and the IPB98 (H-mode) scaling [6]. The optimal agreement between experiment and simulations (using l_i and flux consumption as criterion) with this model in our current ramp-up dataset is obtained using either $H_{96-L} = 0.6$ or $H_{IPB98} = 0.4$. Interestingly, the energy confinement time during current ramp-up phases of selected DIII-D and C-MOD discharges (not included in the validation dataset yet) follow approximately the same H factors, which strengthens the confidence in this scaling-based approach.
- The empirical Bohm/gyro-Bohm model, in its original L-mode version without magnetic shear dependence [7].
- The Coppi–Tang model [8]
- The GLF23 model [9], applied either up to the LCFS ('GLF23 full rad.' in figures) or substituted by a constant diffusion coefficient of $8\,m^2\,s^{-1}$ in the edge region $0.8 < \rho < 1$ ('GLF23 $\rho < 0.8$' in figures), see below for the motivation for this substitution

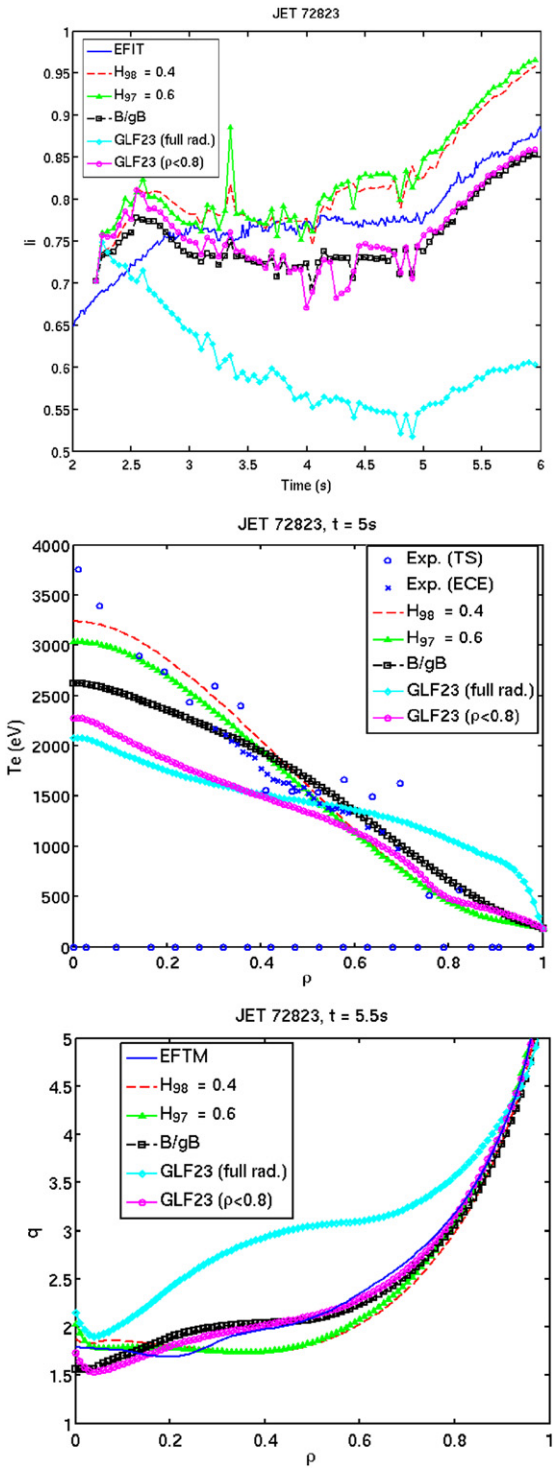

Figure 4. Top: simulation of the internal inductance dynamics of a JET LHCD assisted current ramp-up (2 MW of LHCD applied + 1.5 MW NBI diagnostic beam) with several heat transport models. The plasma current is ramped up to 1.15 MA in 5 s. The same colour code as in figure 2. Middle: the electron temperature profile at $t = 5$ s. Bottom: the q-profile at $t = 5.5$ s, in comparison with MSE constrained equilibrium reconstruction (blue, 'EFTM').

Figures 1–6 present some typical highlights of this comparison of the models with experimental data, which

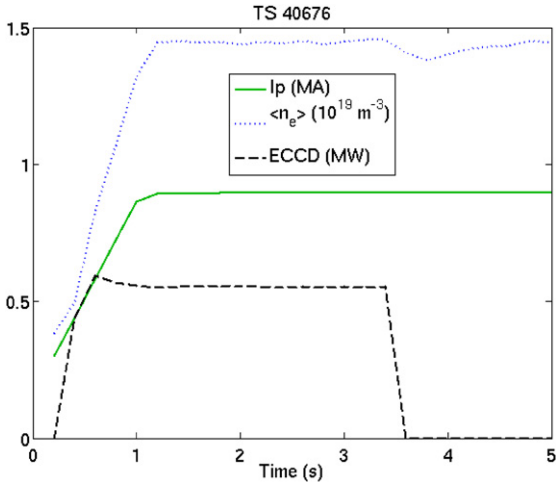

Figure 5. Scenario of Tore Supra shot #40676 (ECCD). Time traces of plasma current I_p (green, solid), volume-averaged electron density $\langle n_e \rangle$ (blue dots), ECCD power (black dash).

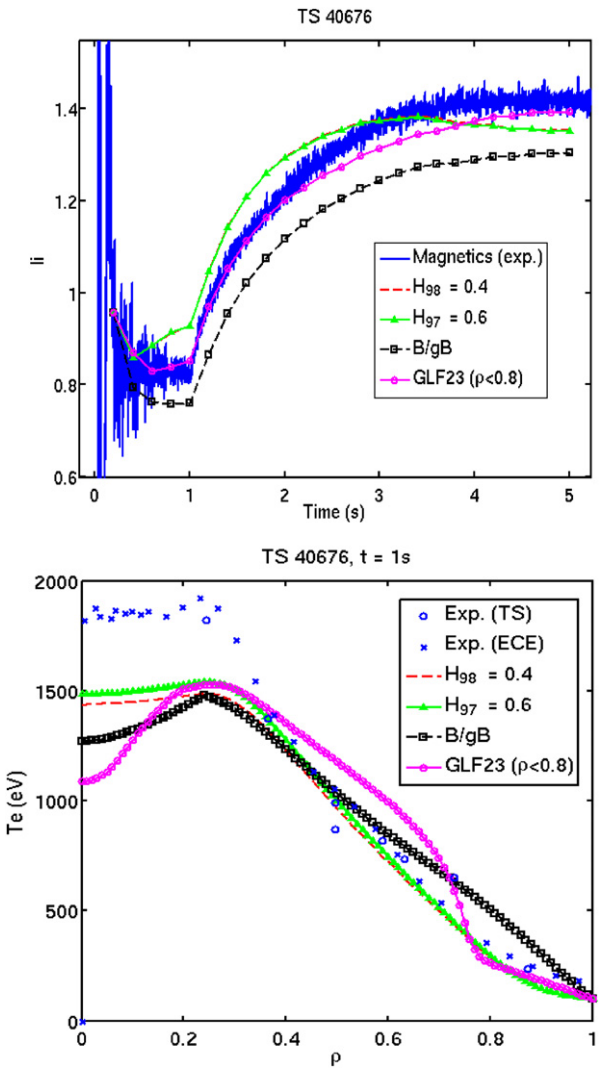

Figure 6. Top: simulation of the internal inductance dynamics of a Tore Supra ECCD assisted current ramp-up (co-ECCD applied at $\rho = 0.3$) with several heat transport models. The plasma current is ramped up to 0.9 MA in 1 s. The same colour code as in figure 2. Bottom: the electron temperature profile at $t = 1$ s.

Table 2. Tore Supra shot #40676. Time of occurrence of the first sawtooth in experiment (2st column) and of occurrence of the $q = 1$ surface in the simulations with various models.

	Exp.	BgB	GLF23 ($\rho < 0.8$)	Scaling $H_{98} = 0.4$	Scaling $H_{97} = 0.6$
T($q = 1$) [s]	2.4	3.1	2.7	2.3	2.3

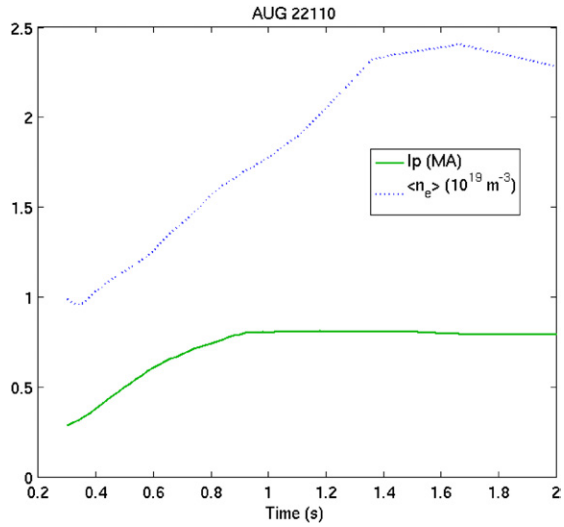

Figure 7. Scenario of AUG shot 22110 (ohmic). Time traces of plasma current I_p (green, solid) and volume-averaged electron density $\langle n_e \rangle$ (blue dots).

includes both ohmic and discharges with moderate heating during the current ramp-up. On the JET ohmic discharge #71827 the Bohm/gyro-Bohm and the GLF23 with edge substitution models are most accurate in T_e and l_i while the scaling-based models tend to slightly overestimate T_e in the core (figures 1 and 2). However, this behaviour is not general. The Coppi–Tang model grossly overestimates the electron temperature and l_i.

For the JET discharge #72823, which features 2 MW of lower hybrid current drive (LHCD) and 1.5 MW of neutral beam injection (NBI, diagnostic beam) the Bohm/gyro-Bohm and scaling-based models describe the l_i and electron temperature dynamics with the same satisfying accuracy (figures 3 and 4). In this discharge, LHCD has an important influence on the l_i and T_e dynamics in the current ramp-up and must be carefully modelled. The optimal reconstruction of the experimental data here is obtained by a significant ad hoc broadening of the LH power deposition and current drive profiles with respect to the results of the used LHCD solver (DELPHINE ray-tracing/Fokker–Planck solver within CRONOS) [10, 11]. The need for this ad hoc broadening, which appears frequently when carrying out a detailed comparison with experimental data (see e.g. [11]), could be due to LH physics elements missing in this simulation, such as (i) taking into account the full launched power spectrum (as a function of the parallel refractive index) instead of a simple two lobes description, (ii) taking into account the scattering of LH waves induced by density fluctuations. Using this broadening procedure and depending on the transport model, the target q-profile at the end of the current ramp-up can be reconstructed within 0.5 accuracy with respect to a

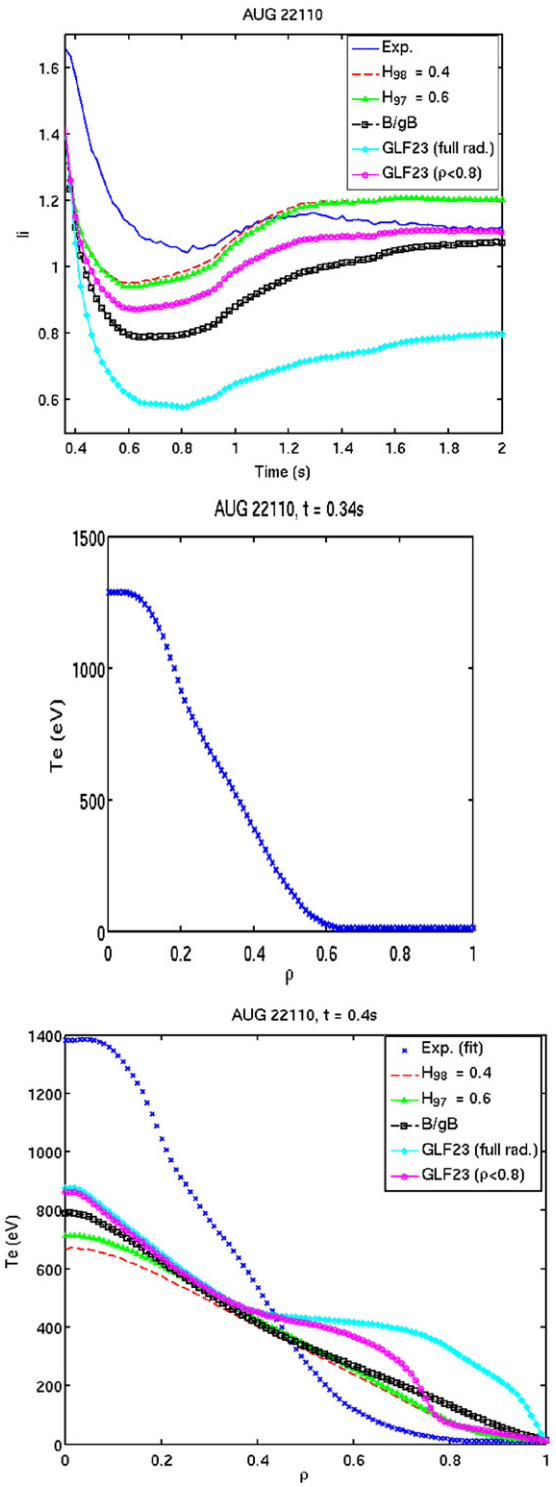

Figure 8. Top: simulation of the internal inductance dynamics of an AUG ohmic shot with several heat transport models. The plasma current is ramped up to 0.8 MA in 0.9 s. The same colour code as figure 2. Middle: electron temperature profile at $t = 0.34$ s (fitted from measurements). Bottom: electron temperature profile at $t = 0.4$ s.

motional Stark effect and magnetic measurements constrained equilibrium reconstruction (figure 4, bottom).

Using the first-principles based GLF23 model in the current ramp-up phase is a challenge, in particular because

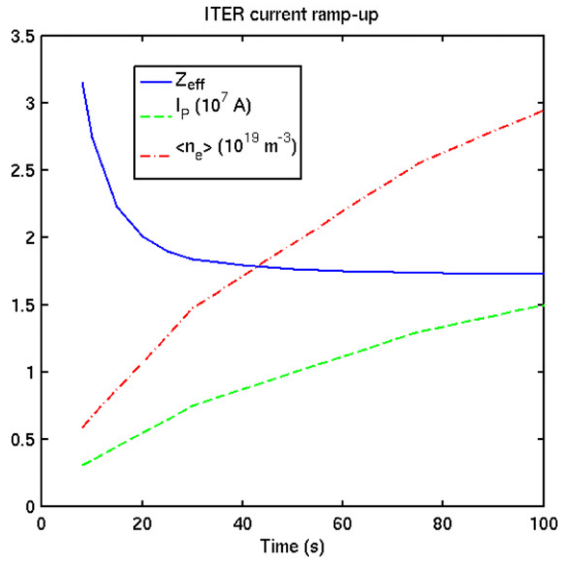

Figure 9. Main reference time traces for the simulations of ITER current ramp-up. Effective charge $Z_{\rm eff}$ (blue, solid), plasma current (green, dash) and volume-averaged electron density (red, dashed–dotted). In the case with ECRH, 20 MW ECRH are applied from $t = 30$ s up to the end of the current ramp ($t = 100$ s).

our figure of merit (the accuracy in predicting the internal inductance) is strongly weighted by what happens in the outer half of the plasma. When applied up to the LCFS, the GLF23 model tends to predict a very low level of transport, resulting in a sort of pedestal in $T_{\rm e}$, which is not consistent with the experimental data and leads to a strong underestimation of $l_{\rm i}$ (figures 4 and 8). This behaviour seems to be general on our dataset and is a major caveat for the application of GLF23 in the ramp-up phase. In order to correct this problem, the model has been arbitrarily patched in the region $0.8 < \rho < 1$ by prescribing a fixed diffusion coefficient $\chi_{\rm e} = \chi_{\rm i} = 8\,{\rm m}^2\,{\rm s}^{-1}$. With this patch, GLF23 provides rather accurate $l_{\rm i}$ and $T_{\rm e}$ dynamics on the JET shots, though still has problems reproducing the $T_{\rm e}$ profile on Tore Supra.

For the Tore Supra case (figures 5 and 6), the scaling-based models are the most accurate in terms of electron temperature. As a consequence they are also the most accurate for correlating the time of occurrence of the first sawtooth in experiment and the occurrence of the $q = 1$ surface in the simulations (see table 2).

The AUG discharge in our dataset (figures 7 and 8) is not reproduced as well by the models so far. The reason is most probably that the outer third of this discharge is impurity dominated (unboronized machine) and a careful treatment of the radiated power must be applied in the simulation. The outer part of this plasma is strongly cooled by radiation, so that $T_{\rm e}$ is still below 50 eV in the region $0.6 < \rho < 1$ at $t = 0.34$ s. This region of surprisingly low $T_{\rm e}$ for confined tokamak plasmas gradually reduces as the current is ramped-up but still covers $0.8 < \rho < 1$ at $t = 0.5$ s (already half of the flat-top plasma current has been ramped-up). Without a proper treatment of this quite peculiar situation in terms of radiated power, our simulations cannot capture such dynamics and predict higher temperature in the outer half of the plasma, thus delaying the current penetration and underestimating $l_{\rm i}$. Eventually, during the current flat-top, the scaling-based and Bohm/gyro-Bohm

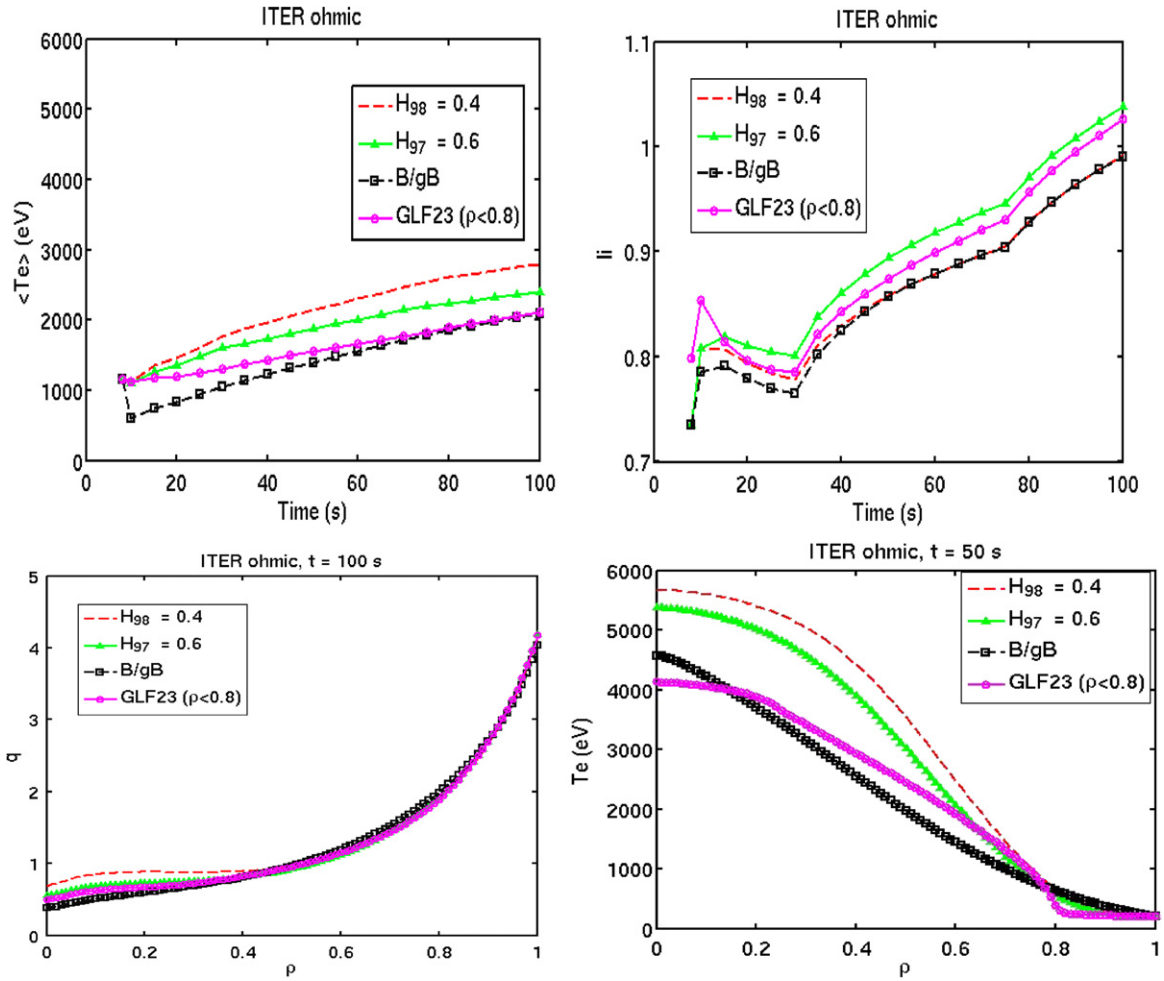

Figure 10. Simulations of ITER current ramp-up in an ohmic case, using the following heat transport models: scaling-based ($H_{98} = 0.4$, red dash), scaling-based ($H_L = 0.6$, green triangles), Bohm/gyro-Bohm (black squares), GLF23 (applied only inside $\rho = 0.8$ with $\chi_e = \chi_i = 8\,m^2\,s^{-1}$ outside, purple). Top: time traces of the volume-averaged electron temperature (left) and internal inductance (right). Bottom: the q-profile at the end of the current ramp (left), the electron temperature profile at the middle of the current ramp (right).

models recover a relatively accurate prediction of the electron temperature profile and of the l_i value within the previous error bar of ± 0.15.

The main conclusion of this study is that the Bohm/gyro-Bohm and scaling-based models are the most accurate ones for modelling the L-mode current ramp-up phase of at least two different tokamaks, yielding on our dataset (but the AUG radiation dominated discharge) the correct l_i dynamics within ± 0.15.

2.2. *Projections to ITER*

Using the most accurate transport models (Bohm/gyro-Bohm and scaling-based), projections to the ITER current ramp-up phase are carried out. The GLF23 model with edge substitution is also used for comparison, though we do not recommend its use for extrapolation to ITER owing to the arbitrariness of the $\chi_e = \chi_i = 8\,m^2\,s^{-1}$ substitution. In these simulations the plasma current is ramped up to 15 MA in 100 s (figure 9). An ohmic case and an ECRH case are presented (in the latter case, 20 MW of ECRH are added at mid-radius from $t = 30$ s onwards). The plasma LCFS is prescribed to a constant D-shape throughout the simulation. Figures 10 and 11 display the dynamics of the internal inductance, the q-profile at the end of the ramp ($t = 100$ s) and the electron temperature profile at the middle of the ramp ($t = 50$ s) for the various transport models. Although significant differences between models appear on the electron temperature prediction (in particular, inside the ECRH deposition in the ECRH case), the final q-profiles reached at the end of the ramp are rather close (for a given heating scheme). The difference between models on the $l_i(3)$ prediction is also small, of the same order as for the present experiments, i.e. ± 0.1. Thus, even in an ITER case with a strong and narrow heating source, all selected transport models behave rather similarly in terms of l_i dynamics and target q-profile, providing a prediction envelope which, for the experimental validation dataset contained the experimental value. As expected, the addition of ECRH during the current ramp delays the current penetration due to the decrease in the plasma resistivity with increasing electron temperature, with respect to the ohmic case. The internal inductance is lower by typically 0.05–0.15, which is significant owing to the rather narrow l_i operating space of the ITER PF systems [12]. While the target q-profile at $t = 100$ s is monotonic and sawtoothing in the ohmic case (sawtoothing was not included in the simulations), it is just above 1 and slightly hollow in the

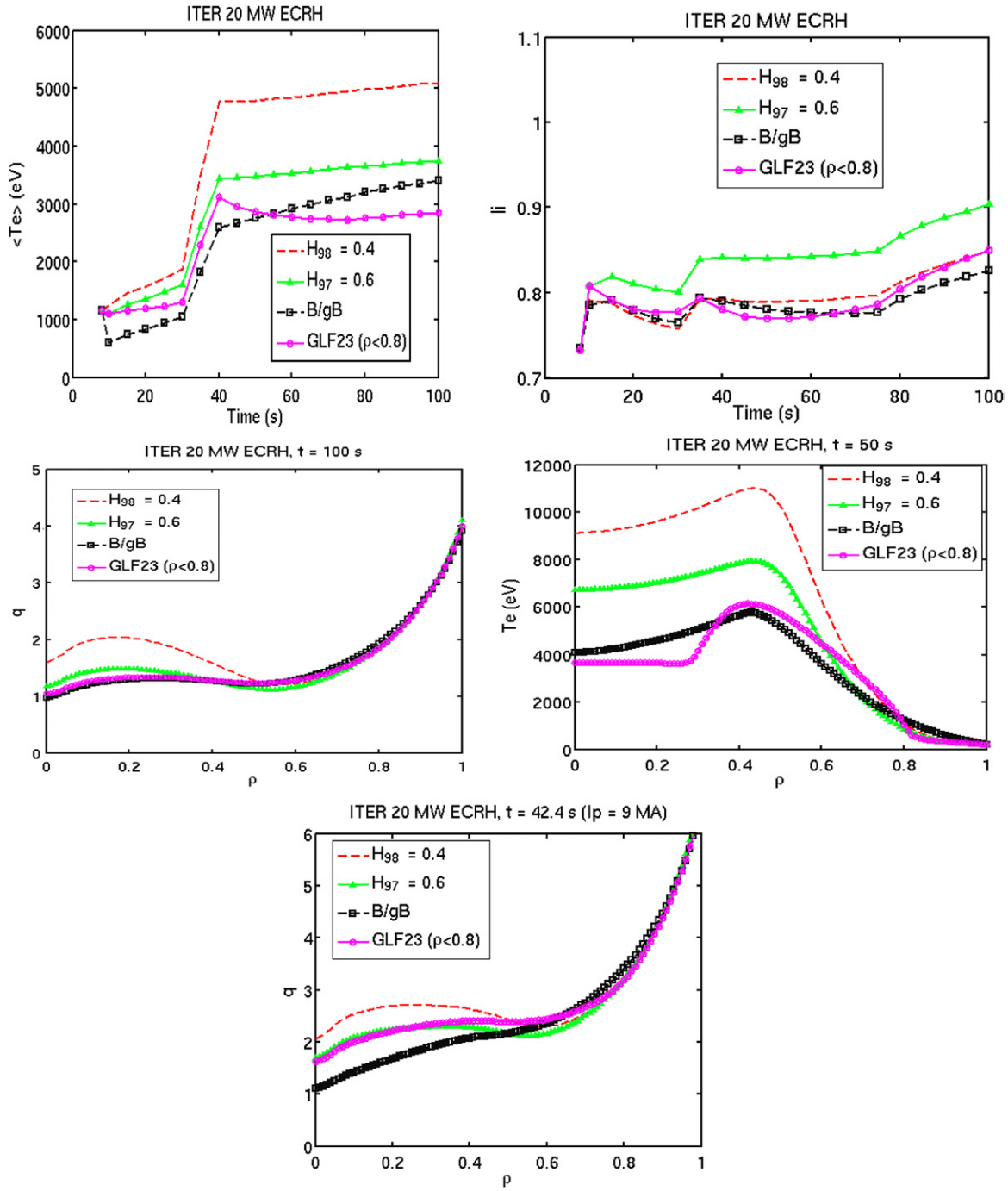

Figure 11. Simulations of ITER current ramp-up in an ECRH case (20 MW of ECRH are added at mid-radius from $t = 30$ s onwards), using the same models and colour codes as in figure 10. Top: time traces of the volume-averaged electron temperature (left) and internal inductance (right). Middle: the q-profile at the end of the current ramp (left), the electron temperature profile at the middle of the current ramp (right). Bottom: the q-profile when I_p reaches 9 MA, shown for comparison with the expected target q-profile of ITER steady-state scenario.

ECRH case. Earlier during the current ramp, when I_p reaches 9 MA at $t = 42.4$ s, the q-profile with the scaling-based models is slightly reversed in the ECRH case with a local minimum around $q = 2$, i.e. close to the target q-profile expected for the ITER 'steady-state' scenario. This target q-profile control capability (also available with other electron heating schemes such as LHCD [10]) will be useful in view of carrying out advanced scenarios ('hybrid' or 'steady-state') on ITER, which may require starting the main heating phase without the $q = 1$ surface being in the plasma. These trends in the comparison between the ECRH and ohmic cases are obtained with all of the transport models retained in our selection.

In the simulations above, none of the used empirical models accounts for the internal transport barrier (ITB) (the model GLF23 potentially takes ITBs into account but does not trigger one here). When using the CDBM model,

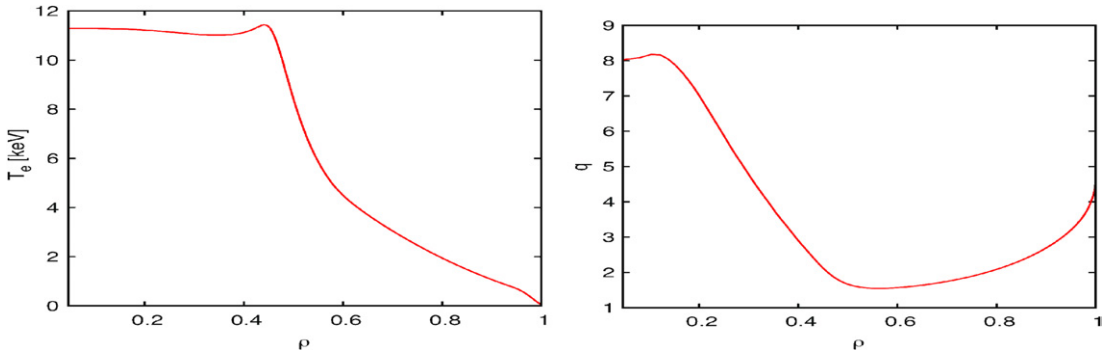

Figure 12. Projection of the ITER current ramp-up phase in case 20 MW of ECRH are added at mid-radius early from $t = 10$ s onwards (flat-top value $I_p = 15$ MA reached at $t = 70$ s). The dynamic evolution of plasma expansion is solved by the TSC code with the CDBM transport model. Electron temperature (left) and q-profile (right) at the end of the current ramp.

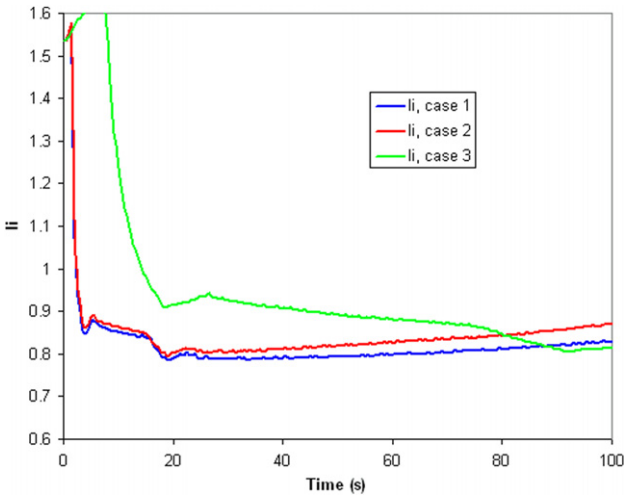

Figure 13. Sensitivity analysis in the ohmic ITER ramp-up case (flat-top value 15 MA reached at $t = 100$ s) with the scaling-based model $H_{98} = 0.4$. Case 1 (blue): constant $Z_{eff} = 1.7$, T_{ea} ramped up from 25 to 250 eV. Case 2 (red): constant $Z_{eff} = 1.7$, T_{ea} 25–100 eV. Case 3 (green): Z_{eff} ramped down from 4 to 1.7, T_{ea} 25–250 eV.

which well reproduces a JT-60U reversed-shear discharge [13], ECCD applied at mid-radius during the ITER current ramp-up triggers an ITB, delaying further the current penetration inside mid-radius and yielding a strongly reversed target q-profile (figure 12).

Those projections are documented with sensitivity analysis. Indeed the absolute value of l_i and its dynamics depend on physical parameters that are given when analysing present experiments but which have to be assumed in the case of projection to ITER. These are effective charge, initial conditions, boundary conditions for the transport equations, plasma shape and last but not least electron density. Figure 13 presents such a sensitivity analysis on T_e boundary condition T_{ea} and Z_{eff} dynamics in the case of the ohmic ITER ramp-up introduced at the beginning of this section and using the scaling-based model with $H_{98} = 0.4$. The impact of the T_{ea} variation is relatively small (less than 0.05 in l_i at the end of the I_P ramp-up), while using high Z_{eff} at the beginning of the current ramp-up makes a quite strong difference in l_i during the early phase, which eventually disappears at the end of the ramp-up.

3. Integrated simulations of ITER current ramp-down

Figure 14 illustrates two possible ITER fast current ramp-down scenarios, simulated by the Astra code [14], one with an H–L back transition (left), the other maintaining the plasma in H-mode with the use of higher heating power (right). The main challenge with the H–L back transition is the sudden drop in pressure (see β_P in the figure), which may cause a significant inward shift of the plasma and contact to the wall. Conversely the scenario of plasma termination in H-mode has no significant drop in β_P, but features a large increase in l_i at the end of the discharge which could cause vertical instability when I_P reaches 3 MA.

The fact that the plasma energy content changes so rapidly after the H–L transition points to the importance of a self-consistent simulation of plasma equilibrium using free-boundary equilibrium solvers, together with the core transport equations and PF systems controller. Figure 15 shows one example of such a simulation carried out with JETTO and CREATE-NL [15], which was applied to an extract from scenario 2 plasma containing both L–H and H–L transitions. Although the presently adopted ITER shape control system can cope with both L–H and H–L transitions, the latter can push plasma onto the inner limiter when the plasma energy content exceeds level of $W_{th} > 350$ MJ. Successful self-consistent simulation of ITER current ramp-down scenario with DINA-CH coupled to the CRONOS Integrated Modelling code can be found in [16].

Together with the plasma current, the plasma density must also be ramped down without causing excessive divertor power load and while controlling divertor detachment. Using a simple model of edge/core fuelling control, TSC simulations of the ramp-down from ITER burning flat-top were performed on ITER 15 MA/200 s termination scenario. The TSC [17], comprised of two-dimensional free-boundary plasma equilibria and one-dimensional transport model (CDBM), describes time-evolution of the plasma shape and profile dynamics of the plasma current I_p and temperature as well as density. The plasma density was controlled by feedback on neutral gas puff from the edge and core fuelling like pellet injection. Two ramp-down scenarios have been studied, one keeping the edge/core fuelling control invariant ($f_{edge/core} = 0.8$, i.e. 80% of fuel particles is supplied by gas puffing

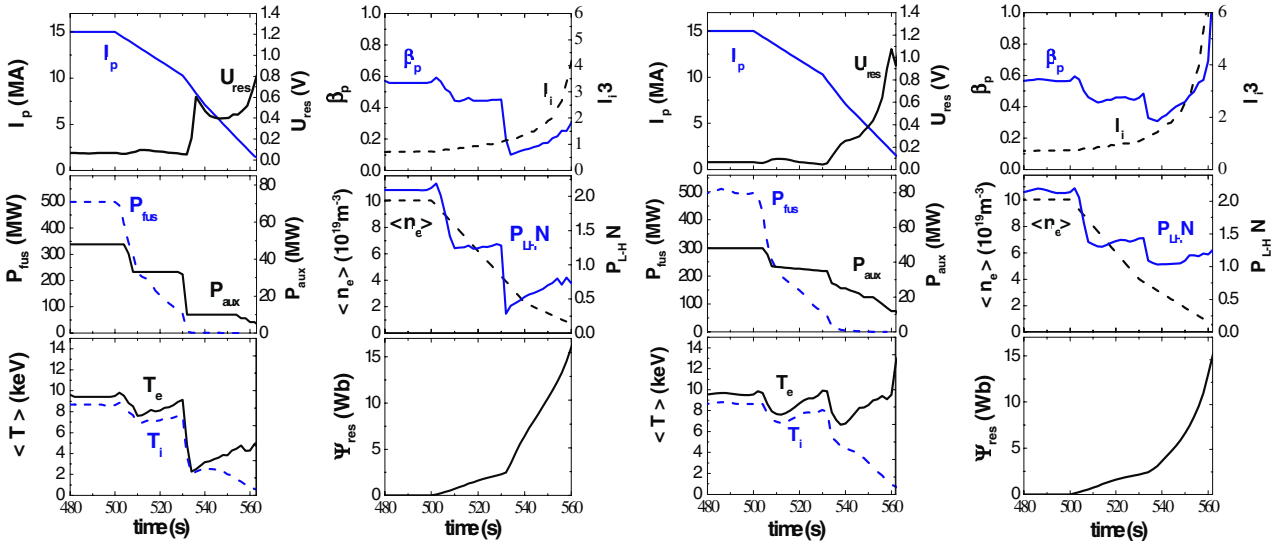

Figure 14. Plasma termination scenarios in L-mode (left, H–L transition triggered at $t = 530$ s by decreasing the additional power P_{aux}), and staying in H-mode (right), simulated with the Astra code.

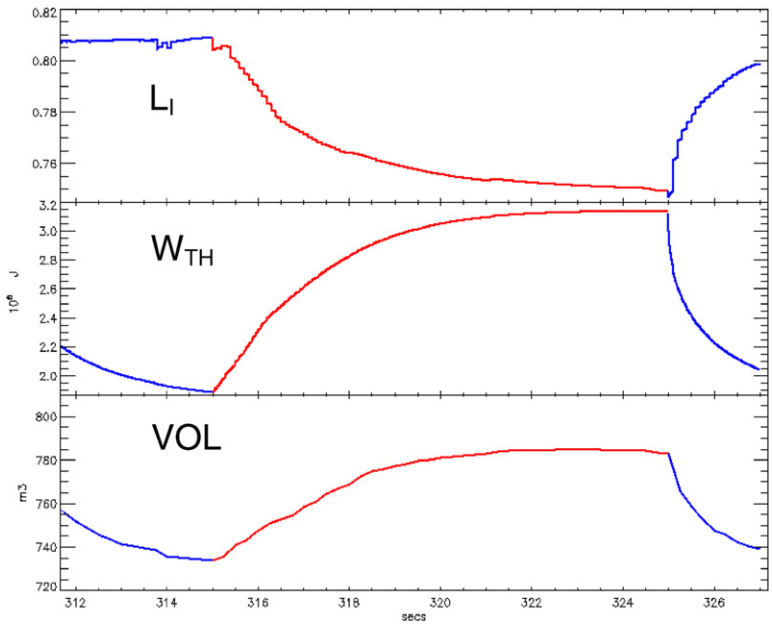

Figure 15. From top to bottom: internal inductance (plasma is in L-mode when colour is blue and in H-mode when colour is red), plasma thermal energy content and plasma volume.

while 20% by core fuelling, figure 16 left), in the other $f_{\mathrm{edge/core}}$ is ramped down linearly from 0.8 at 500 s to 0.0 (totally core fuelling) at $t = 600$ s (figure 16 right). Time-evolution of divertor neutral pressure p_0 was solved by a zero-dimensional model of particle flux from and to the core plasma, accumulation and pumping-out dynamics of fuelling gas without consideration of wall pumping and retention. The H–L mode transition was forced at 600 s. Figure 16 shows the dynamics of some of the SOL/divertor parameters, which are quite different depending on the fuelling scenario. It thus follows that edge/core fuelling control during the termination of ITER discharge is a key operating instruction for a slow and safe density ramp-down from high-Q burning flat-top.

4. Conclusions

Over the past two years, significant modelling efforts have been carried out throughout the world to simulate the current ramp-up and ramp-down phases of the 15 MA ITER reference scenario. In particular, a set of empirical heat transport models for L-mode (namely the Bohm–gyroBohm model and scaling-based models with a specific fixed radial shape and $H_{96\text{-L}} = 0.6$ or $H_{\mathrm{IPB98}} = 0.4$) has been validated on a multi-machine experimental dataset for predicting the l_{i} dynamics within ± 0.15 accuracy during current ramp-up and ramp-down phases. Simulations using the Coppi–Tang or GLF23 models (applied up to the LCFS) overestimate or underestimate the internal inductance beyond this accuracy

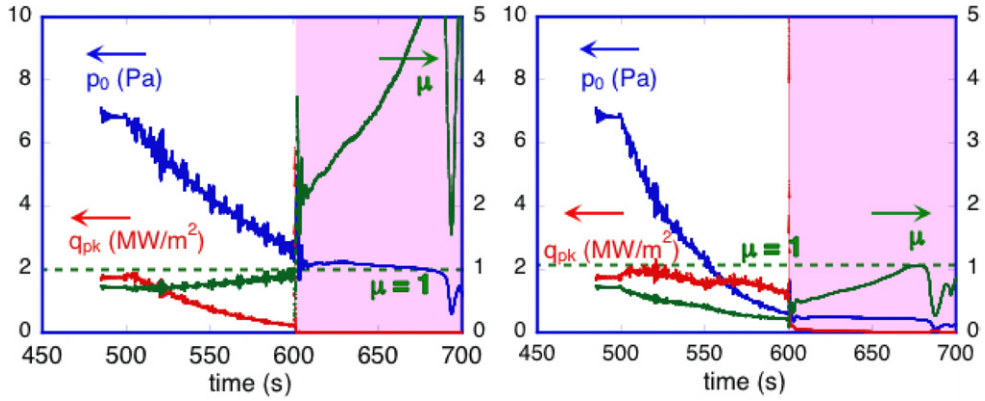

Figure 16. Left: simulation of the divertor power load q_{pk}, the normalized neutral pressure μ and the divertor neutral pressure p_0, keeping the edge/core fuelling control invariant ($f_{edge/core} = 0.8$). Right after H–L transition at 600 s, the operating point of inner divertor becomes strongly detached ($\mu \gg 1$). Right: simulation of q_{pk}, μ and p_0, changing $f_{edge/core}$ from 0.8 at 500 s to 0.0 (totally core fuelling) at 600 s. Even after H–L transition, the operating point of inner divertor remains attached in 'regime A' ($\mu < 1$), though a higher heat pulse of more than 10 MW m^{-2} arises at the H–L transition.

(more than ± 0.2 discrepancy in some cases). The ± 0.15 accuracy on l_i is obtained using the density profile peaking and the electron temperature boundary condition (at the LCFS) from the experiment, which of course is not possible for present extrapolations to ITER. Therefore the sensitivity of the predictions using these models has been quantified when applied to ITER current ramp-up simulations. Of course, the validity of extrapolating such empirical models from present devices to ITER can be questioned, precisely because they are empirical. The multi-machine approach adopted in the validation exercise (as well as in the scaling approach underlying some of the models) answers this partially. The difficulties of applying first-principles based transport models, such as GLF23 in the outer zone of the plasma $\rho > 0.8$, have been shown. This makes such models difficult to use in view of predicting the l_i dynamics.

Integrated modelling can now address operational aspects of the current ramp-up and ramp-down phases of ITER scenarios. This involves coupled free-boundary equilibrium solvers, the core transport code and PF systems circuit equations, including voltage controller, in order to test the capability of the ITER PF systems to handle the chosen scenario. The H–L back transition at the end of the burn is one of the challenging phases of the operation that must be prepared by such complex integrated simulations. Another challenging aspect is the modelling of the plasma breakdown, which sets the initial conditions prior to the current ramp-up. This should also be addressed in the future, probably with dedicated codes and models for describing the specific processes occurring during this phase (pre-ionization, burnthrough, etc). Another key ingredient that should be integrated in the simulations is particle fuelling and transport, including core edge interaction in order (i) to verify that the chosen scenario can indeed be fuelled and (ii) to check the operational limits of the divertor. This work shows recent examples of such highly integrated simulations, which presently are far from routine usage. In the recent years, modelling codes have progressed technically to reach this high level of integration of the usual core transport equations with more and more operational aspects. Nonetheless, a strong effort of validation of the individual models used in these integrated simulations on existing experiments remains the backbone and starting point of any extrapolation procedure and a significant effort has still to be carried out in this area. Dedicated scaled experiments are interesting for this purpose [18]. Ultimately, the developed models and integrated simulators will provide an essential support to the preparation of ITER scenarios and operation.

Acknowledgments

This work was partly supported by EURATOM and carried out within the framework of the European Fusion Development Agreement. The views and opinions expressed herein do not necessarily reflect those of the European Commission. The views and opinions expressed herein do not necessarily reflect those of the ITER Organization.

References

[1] Parail V. *et al* 2009 *Nucl. Fusion* **49** 075030
[2] Pereverzev G.V. and Yushmanov P.N. 2002 *Report* IPP 5/98, Garching
[3] Artaud J.F. *et al* 2010 *Nucl. Fusion* **50** 043001
[4] Cennacchi G. and Taroni A. 1988 *Report* JET-IR(88) 03
[5] Kaye S. *et al* 1997 *Nucl. Fusion* **37** 1303
[6] ITER Physics Basis 1999 *Nucl. Fusion* **39** 2137
[7] Erba M., Aniel T., Basiuk V. Becoulet A. and Litaudon X. 1998 *Nucl. Fusion* **38** 1013
[8] Jardin S.C., Bell M.G. and Pomphrey N. 1993 *Nucl. Fusion* **33** 371
[9] Waltz R.E. *et al* 1997 *Phys. Plasmas* **4** 2482
[10] Kim S. *et al* 2009 *Plasma Phys. Control. Fusion* **51** 065020
[11] Imbeaux F. and Peysson Y. 2005 *Plasma Phys. Control. Fusion* **47** 2041
[12] Kessel C.E. *et al* 2009 *Nucl. Fusion* **49** 085034
[13] Takei N. *et al* 2007 *Plasma Phys. Control. Fusion* **49** 335
[14] Leonov M. *et al* 2010 *37th EPS Conf. on Plasma Phys. Control. Fusion (Dublin, Ireland)* P-2.182
[15] Albanese R., Mattei M., Calabrò G. and Villone F. 2003 Unified treatment of forward and inverse problems in the numerical simulation of tokamak plasmas *Int. Symp. on Applied Electromagnetics and Mechanics ISEM 2003 (Versailles, France)*
[16] Kim S.H. *et al* 2009 *Plasma Phys. Control. Fusion* **51** 105007
[17] Kessel C.E. *et al* 2007 *Nucl. Fusion* **47** 1274
[18] Jackson G.L. *et al* 2010 *Phys. Plasmas* **17** 056116